International Journal of Nanomedicine

Dovepress
Taylor & Francis Group

Open Access Full Text Article

ORIGINAL RESEARCH

Highly Stable Antitumor Silver-Lipid Nanoparticles Optimized for Targeted Therapy

Ammar Darwish[1], Nikolett Sándor[1], Imre Szenti[2], Tamás Marosvölgyi[3], Kata Juhász[1], Andrea Rónavári[2], Edi Kachal[2], Bence Kutus[4], Zoltán Kónya[2], Zsolt Balogi[1]

[1]Institute of Biochemistry and Medical Chemistry, Medical School, University of Pécs, Pécs, H-7624, Hungary; [2]Department of Applied and Environmental Chemistry, University of Szeged, Szeged, H-6720, Hungary; [3]Institute of Bioanalysis, Medical School, University of Pécs, Pécs, H-7624, Hungary; [4]Department of Molecular and Analytical Chemistry, University of Szeged, Szeged, H-6720, Hungary

Correspondence: Zsolt Balogi, Email zsolt.balogi@aok.pte.hu

Background: Silver nanoparticles (AgNPs) have a broad spectrum of biocidal effects, allowing also their antitumor application. To enhance bioavailability, minimize adverse effects and enable targeted drug delivery AgNPs may be encapsulated in liposomes. In this study we aimed to create highly stable and effective antitumor AgNP lipid formulations (LAgs).

Methods: Uncapped and citrate-stabilized AgNPs were encapsulated by the lipid film hydration method using several phospholipid mixtures, followed by the essential removal of unencapsulated AgNPs by size exclusion chromatography (SEC). Purified LAgs were characterized by UV-VIS, DLS, XRD, ICP-MS, transmission electron microscopy (TEM) and glycerol-based density gradient centrifugation (DGC). Liposomal stability was assessed by carboxyfluorescein (CF) leakage, while antitumor effects of purified LAgs were tested in MTT, clonogenic and 3D spheroid invasion experiments.

Results: The presence of AgNPs inside SEC-purified liposomes was confirmed by TEM, XRD and ICP-MS. Encapsulation efficiency was estimated to be between 18.7 and 25.5%. Purified LAgs had higher density as compared to free AgNPs revealed by DGC, indicating that a considerable fraction of liposomes contained AgNPs. LAgs with PC/PG, PC/PG/SM/Chol, and in particular PC/PG/SM displayed the highest stability assessed by CF leakage, whereas high content of neutral or negatively charged phospholipids was destabilizing. As shown by MTT and colony formation assays, viability and survival of A375 and RPMI-7951 melanoma cells were severely impaired by LAgs at a higher or comparable level as caused by free AgNPs. Used as a non-tumor control, HEK293 cells were less vulnerable to LAgs as compared to free AgNPs. Finally, applying the most stable lipid composition, PC/PG/SM-LAg-c, and in part PC/PG/SM-LAg-u effectively inhibited a tissue-like invasion of melanoma spheroids.

Conclusion: Altogether, highly stable purified LAg formulations were created, which effectively block survival, clonogenic potential and invasion of melanoma cells, therefore could be promising NP platforms for targeted tumor therapy.

Keywords: silver nanoparticle, liposome, encapsulation, tumor cell viability, tumor spheroid invasion

Introduction

Nanoparticles (NPs) have gained significant attention in modern medical science for their potential in both treatment and diagnosis due to their small size, easy penetration through barriers as well as their tunable surfaces that enable selective targeting.[1] NPs represent a promising alternative to macromolecule-based drugs that have severe limitations in biomedical applications.[2] Silver nanoparticles (AgNPs) are metallic NPs that are known for their optical and versatile biocidal properties.[3] They show unique antimicrobial features against a wide range of both Gram-positive and -negative bacteria without provoking microbial resistance, therefore could be considered a perfect surrogate for antibiotics and are also involved in wound dressings.[4,5] AgNP efficacy is not confined to bacteria as numerous reports highlighted their antiviral and antifungal activities.[6,7] AgNPs are believed to exert these effects by either provoking redox imbalance by the excessive production of reactive oxygen species (ROS) or by releasing Ag^+ from NPs.[8] Several studies have revealed the intrinsic antineoplastic ability of AgNPs against various cancer cell lines in both in vitro and in vivo mouse models, as applying AgNPs resulted in tumor regression and increased survival.[9,10] Furthermore, when applied in combination,

Received: 27 September 2024
Accepted: 21 December 2024
Published: 1 February 2025

AgNPs intensified the anticancer effect of chemotherapeutic agents.[11] It has been suggested that AgNPs employ their cytolytic effect through the release of Ag^+ in the acidic endo-lysosomal system, followed by lysosomal membrane permeabilization and free radical accumulation, leading to cell death. AgNPs may also distort the cellular membrane by provoking lipid peroxidation, by which AgNPs can enter the cell, resulting in oxidative stress-mediated cytotoxicity.[12–14] Additional mechanisms of AgNP cytotoxicity may include direct interaction with and depletion of thiol-containing glutathione,[15] DNA damage in the nucleus,[16] or upregulation of p53.[17] An antiangiogenic activity of AgNPs has been shown to be paralleled with the suppression of hypoxia-inducible factor-1 and its downstream gene vascular endothelial growth factor-A.[18]

Despite the broad spectrum of AgNP effects, their direct biomedical application is hampered by several factors. The mononuclear phagocyte system (MPS) recognizes AgNPs as foreign particles and sequesters them in the liver and other organs. This greatly reduces AgNP bioavailability at the tumor site and causes adverse effects in off-target organs.[19] AgNPs also can cause hemotoxic effects as shown by their ability to trigger hemolysis and lymphocyte inhibition.[20] Additionally, AgNPs may interfere with platelet function by inhibiting their aggregation.[21] Furthermore, several in vitro and in vivo studies pointed out toxic effects of AgNPs on healthy mammalian cells as well.[22] Meanwhile, the interaction of AgNPs with components of various biofluids reduces their stability, which negatively affects their cytotoxic effects.[16,23] In fact, our current understanding on the biosafety and toxicity of AgNPs does not allow their clinical applicability.[24] All these drawbacks could be overcome by entrapment of AgNPs in organic coating layers (polymeric micelles, dendrimers, silica nanoparticles),[25] or by encapsulation in lipid-based nanostructures such as liposomes. Liposomes have superior biocompatibility, tunable surfaces, and allow the encapsulation of both hydrophilic and hydrophobic drugs enabling their application in a combination.[26] Liposomes are also biocompatible and low immunogenic due to their composition and cell-like structure.[27] In addition to these benefits, their high targeting potential makes liposomes a preferred candidate for drug delivery into tumors.[28] Several reports pointed out the benefits of encapsulating metallic NPs inside liposomes. Entrapment of superparamagnetic iron oxide NPs in liposomes has been shown to improve the sensitivity of magnetic particle imaging.[29] Additionally, in a recent biophysical study it has been suggested that LAgs made of cholesterol and phosphatidylcholine (PC) release their AgNP content at more acidic pH present in tumor tissues and intracellular endolysosomal compartments.[30] Furthermore liposomal encapsulation of AgNPs may allow controlled release and prolonged toxic effects.[31] Using liposomes as carriers of AgNPs, only a handful of studies tested antineoplastic effects, and only on 2D cell cultures.[32–34] In these studies, LAg formulations were not purified from free, unencapsulated AgNPs, therefore the pure effect of LAgs could not be revealed. Even though a general beneficial effect of the liposomal formulation of AgNPs, other than avoiding unwanted toxicity, could be expected, this still needs to be tested using purified LAgs of varying lipid composition. The above studies used a previously established liposome formulation made of dipalmitoyl/ distearyl-PC (DPPC/ DSPC) and cholesterol,[35] which is supposed to have low MPS recognition.[36] However, in the original biophysical study it was shown that hydrophobic AgNPs were incorporated into the lipid bilayer, by which oversized AgNPs considerably perturbed the membrane structure, greatly reducing the lipid phase transition temperature and increasing fluidity. These overall changes, in fact, impair the physicochemical advantages of DPPC/cholesterol liposomes, which may then undermine the possible biomedical use of this lipid formulation as AgNP carrier. Inspired by these challenges towards future medical use of AgNPs, we intended to perform a systematic study to characterize a series of purified LAgs and identify those with superior physicochemical properties, in particular stability. On the way towards active tumor targeting with LAgs, we also aimed to test the passive, untargeted antitumor effects of the most stable LAgs on viability, clonogenic survival as well as on a tissue-like 3D tumor spheroid invasion.

Methods

Preparation of Silver Nanoparticles

Uncapped AgNPs

Uncapped AgNPs were prepared by the chemical reduction of silver nitrate (AgNO3) (Sigma Aldrich, USA) using sodium borohydride (NaBH4) (Sigma Aldrich, USA) as reported by Badawy et al[37] with a little modification. Shortly,

30 mL of 2 mm NaBH4 was stirred in an ice bath, then 8 mL of 5 mm AgNO3 was added dropwise under vigorous stirring. The solution turned brownish, indicating the formation of AgNPs. Then it was equilibrated at room temperature.

Citrate-Capped AgNPs

The protocol published by Bélteky et al[38] was followed. Briefly, a 75 mL solution of 9 mm trisodium citrate (TSC) (EMD Millipore, USA) was heated to 75 °C. Then 2 mL of 1% AgNO3 was added to the TSC solution, followed by the dropwise addition of 2 mL of freshly prepared 0.1% NaBH4 solution under vigorous stirring. The resulting yellowish solution was stirred for 1 h and then cooled down to room temperature, followed by dialysis against citrate solution for 24 h.

AgNP Characterization

The formation of AgNPs was checked by recording UV spectra (V-730 Double Beam UV-Visible Spectrophotometer, JASCO Inc., Japan). The hydrodynamic diameter and zeta potential of AgNPs were measured by dynamic light scattering (DLS) measurement using a Zetasizer Nano Instrument (Malvern Instruments, Malvern, UK). Morphology and size were assessed by transmission electron microscopy (TEM) (FEI Tecnai G^2 20 X Twin instrument, FEI Corporate, USA) using carbon film-coated copper grids (CF200-Cu). Size distribution was calculated using ImageJ (National Institutes of Health, USA) and OriginPro 2023b (OriginLab, USA).

Preparation of Liposomes and LAgs

All lipids were purchased from Avanti Polar Lipids, USA. Different formulas of liposomes were prepared using the lipid film hydration technique (Table 1). Lipids (1 mg in total) were mixed at the appropriate molar ratio, then the organic solvents were removed by evaporation under nitrogen flow. To ensure the complete removal of any remaining traces of organic solvents, samples were left under vacuum for 2 h. Large unilamellar vesicles (LUVs) were obtained by hydrating the lipid films using 500 µL distilled water, sonication at 40 °C for 10 min, and repeated extrusion through 100 nm polycarbonate membranes using a LiposoFast-Basic extruder (Avestin, Canada). To prepare Ag-liposomes (LAgs) the same procedure was used, except that distilled water was replaced with AgNP solutions that were in prior filtered with 50 nm polycarbonate membranes.

Liposome Purification

Removal of non-encapsulated AgNPs was performed by size exclusion chromatography (SEC) using Sephadex G-200 (Chemsavers Inc., USA). Briefly, Sephadex G-200 powder was soaked in water for 3 days until complete swelling, then the gel was packed into 1.5×12 cm columns. LAgs were loaded and eluted using distilled water. Fractions containing purified LAgs (2.0 mL in total) were monitored by staining with anilinonaphthalene-8-sulfonic acid (ANS) (Sigma Aldrich, USA) that gives green light under UV in the presence of lipids.

Liposome Characterization

Zeta potential and hydrodynamic diameter were assessed by DLS measurements. TEM was used to visualize LAgs. In short, a drop of LAgs was put onto the copper grid (CF200-Cu) for 1 min and fixed with 2.5% glutaraldehyde for 2 min.

Table 1 Compositions of Different Liposomes Used in This Study

Lipid Composition	**Molar Ratio**
1,2-Dioleoyl-sn-glycero-3-phosphocholine **(DOPC)**	
DOPC/ 1.2-Dioleoyl-sn-glycero-3-phosphoglycerol **(DOPG)**	1/1
DOPC/DOPG/ N-Palmitoyl-D-sphingomyelin **(SM)**	1/1/1
DOPC/DOPG/ Cholesterol **(Cho)/(SM)**	1/1/1/1
DOPC/DOPG/ 1-Stearoyl-2-arachidonoyl-sn-glycero-3-phosphatidylinositol-4,5-bisphosphate **(PIP2)**	40/55/5
DOPC/DOPG/ 1.2-Dioleoyl-sn-glycero-3-phosphoserine **(DOPS)/PIP2**	20/20/55/5

https://doi.org/10.2147/IJN.S498208

Excess amount of the fixing agent was removed, and then uranyl acetate (UA) 0.5% aqueous solution was dropped and left to settle for 1 min. Excess UA was then soaked up, and the grid was dried at room temperature. Samples, where only AgNPs were visualized, were not stained with UA. Samples were examined using a FEI Tecnai G^2 20 X Twin instrument.

X-Ray Diffraction Analysis

The crystal structures of AgNP and LAg samples were analyzed using X-ray powder diffraction (XRD). The measurements were conducted with a Rigaku MiniFlex II powder diffractometer using Cu Kα radiation. Scanning was performed at a rate of 2°/min over a 2θ range of 10° to 80°.

ICP-MS Analysis of Ag Content

Concentration of Ag^+ in the samples was determined by inductively-coupled plasma mass spectrometry (ICP-MS), using an Agilent 7900 instrument. Prior to analysis, the samples were diluted with ultrapure water (Synergy UV purification system, Merck Millipore) as appropriate. Furthermore, cc. HNO3 (Normatom, VWR Chemicals, 1 wt%) and a solution of Y (Aristar, VWR Chemicals, 100 ppb) were added to the samples and used as internal standards for quantitation. Concentrations were calculated based on a 11-point calibration curve ranging from either 0 to 50 ppb Ag^+ or from 0 to 1 ppm Ag^+, using the ion counts of the 107Ag and 109Ag isotopes. The calibration series was prepared from a commercial ICP multielement standard (Aristar, VWR Chemicals). Accuracy of the determined concentrations was estimated to be ± 3.5%.

Density Gradient Centrifugation (DGC)

As an attempt to separate empty liposomes from LAgs four different layers of 100 µL, 200 µL, 200 µL, and 500 µL with different glycerol concentrations of 40%, 20%, 10%, and 5%, were carefully layered on each other, respectively. 150 µL of 5(6)-carboxyfluorescein (CF) (Sigma Aldrich, Czech Republic)-loaded, purified empty liposomes or LAgs (uncapped and citrate-capped) were loaded on the density gradient, and centrifuged at 17,000 g and 4 °C for 1 h. AgNP content of fractions was analyzed by TEM without staining for liposomes with UA.

Lipid Content Determination

Lipid content of DGC fractions was determined as in[39] with slight modifications. Briefly, 100 µL of 1 mg/mL internal standard of C19-0ME in hexane was added to 100 µL of each sample, then mixed with acetyl chloride at 100 °C for 1 h in a 4:1 methanol:hexane mixture with a pyrogallol radical scavenger. The methyl esters formed were determined on a ThermoTrace 1300 GC, using a flame ionization detector, a programmable temperature vaporizing injector module, and H2 carrier gas on an Agilent VF-23ms capillary column. For qualitative and quantitative analysis, the GLC-463 standard mixture (Nu-Check-Prep INC, MI, USA) was used.

Liposome Leakage Assay

LAg stability in biofluids was investigated by measuring the leaking of CF from liposomes at 37 °C over time. Lipid films were hydrated with a mixture of AgNPs and 60 mm CF (self-quenching concentration). Free CF was removed by SEC using Sephadex G-200, and purified LAgs were mixed with either distilled water, Dulbecco's Modified Eagle Medium (DMEM, Biosera, France), or DMEM +20% fetal bovine serum ultra-low endotoxin (FBS, Biosera, France) in a 1:1 dilution. Appropriate fluorescence intensities of the samples kept at 37 °C were monitored over 7 days.

Cell Culture

All cell lines were obtained from the American Type Culture Collection, USA. Melanoma cell lines A375 and RPMI-7951 were cultured at 5% CO2 and 37 °C in DMEM-F12 and DMEM medium supplemented with 5% and 10% FBS, respectively. Human embryonic kidney, HEK293 cells were cultured at 5% CO2 and 37 °C in DMEM medium supplemented with 10% FBS.

Cell Viability Assay

The cytotoxic effect of free AgNPs and LAgs on A375, RPMI-7951 and HEK293 cells was assessed by measuring the ability of cells to reduce 3-(4,5-dimethylthiazol-2-yl)-2,5-diphenyltetrazolium bromide (MTT) to formazan as reported

by Riss et al.[40] Briefly, 5000 cells/100 µL/well were seeded in a 96-well plate, and then AgNPs and purified LAgs of tenfold dilution were applied at equivalent Ag concentrations unless otherwise stated. Cells were allowed to grow for 48 h, then MTT was added to each well followed by 4 h incubation. After washing, dimethylsulfoxide was added to dissolve the dye. The absorbance of formazan was measured at 560 nm using GloMax®-Multi Detection System (Promega Corporation, USA), and cell viability was calculated.

Clonogenic Assay

To measure the colony-forming ability, A375 and RPMI-7951 cells were seeded with a density of 400 and 500 cells/2 mL/well in 6-well plates and incubated for 6 h until their adherence, respectively. AgNPs and LAgs of tenfold dilution were applied at equivalent Ag concentrations. Cultures were left to grow for 11 days, then washed with Dulbecco's phosphate-buffered saline, fixed with 70% ethanol at room temperature for 30 min, and stained with 0.5% crystal violet solution (Sigma Aldrich, India).

3D Spheroid Invasion Assay

For in vitro 3D spheroid invasion experiments 5000 cells/well were plated into 96-well U-bottom plates (Greiner Bio-One, Hungary) pre-coated with poly-HEMA (10 mg/mL, Sigma-Aldrich, St. Louis, MI, USA). 48 h after seeding, 3D spheroids were embedded into 3 mg/mL Matrigel (Growth Factor Reduced w/o Phenol Red, Corning, NY, USA) containing 1% FBS. AgNPs and LAgs of twofold dilution were applied at equivalent Ag concentrations. Brightfield images of spheroids were taken by a Nikon Eclipse inverted fluorescence microscope (Nikon Corporation, Tokyo, Japan) at 4x magnification. Sizes of total and core areas of spheroid cross-sections were measured by Image J. The size of the invasive front was calculated as a difference of total and core values. Spheroid size changes were expressed as relative to the measured data at 0 h (when embedding in Matrigel).

Statistical Analysis

GraphPad Prism (version 8.0, GraphPad Software, San Diego, CA, USA) was used to perform the statistical analysis. One-way ANOVA was used to compare the means of the different groups. Data were presented as mean ± standard deviation. P-value of < 0.05 was considered statistically significant.

Results

AgNP Characterization

Protocols for the preparation of AgNPs involve the chemical reduction of Ag^+ with or without a capping agent that is meant to prevent AgNP aggregation. As we wanted to encapsulate AgNPs, which itself is a way to entrap AgNPs, both uncapped and citrate-capped batches were prepared. AgNPs-u and AgNPs-c showed a surface plasmon resonance (SPR) peak in the UV-Vis spectra, where presence of citrate as a capping agent caused a red shift compared to AgNPs-u (Figure 1A). TEM images directly confirmed that both types of AgNPs have spherical uniform morphology with an average size of 23.3 ±7.8 nm and 6.4 ±1.7 nm for AgNPs-u and AgNPs-c, respectively (Figure 1B). Measured by DLS the hydrodynamic diameter and zeta potential of AgNPs were found to be 45.0 nm and −27.0 mV for AgNPs-u and 32.4 nm and −41.3 mV for AgNPs-c. These values indicated that AgNPs-u are larger and more prone to aggregation as compared to AgNPs-c, but both types of AgNPs appeared suitable for encapsulation into liposome nanocarriers.

Encapsulation of AgNPs in Liposomes

LAgs were prepared using the lipid film hydration method with different lipid compositions (see Table 1), with the expectation that AgNPs could be encapsulated within the liposomal structure. To test the effect of the lipid composition on LAg formation and stability a series of biocompatible or charged lipids were applied. Of these PC, PG, SM and Cho were used as bulk lipids, while PS and PIP2 were involved to test the effect of lipid membrane charges. As the less hydrophilic AgNPs-u were made fairly large (see Figure 1B: 23.3 ±7.8 nm) their incorporation into a 3–4 nm thick liposomal membrane[35] was not possible. AgNPs-c with as low as −41.3 mV Zeta potential were also not likely to

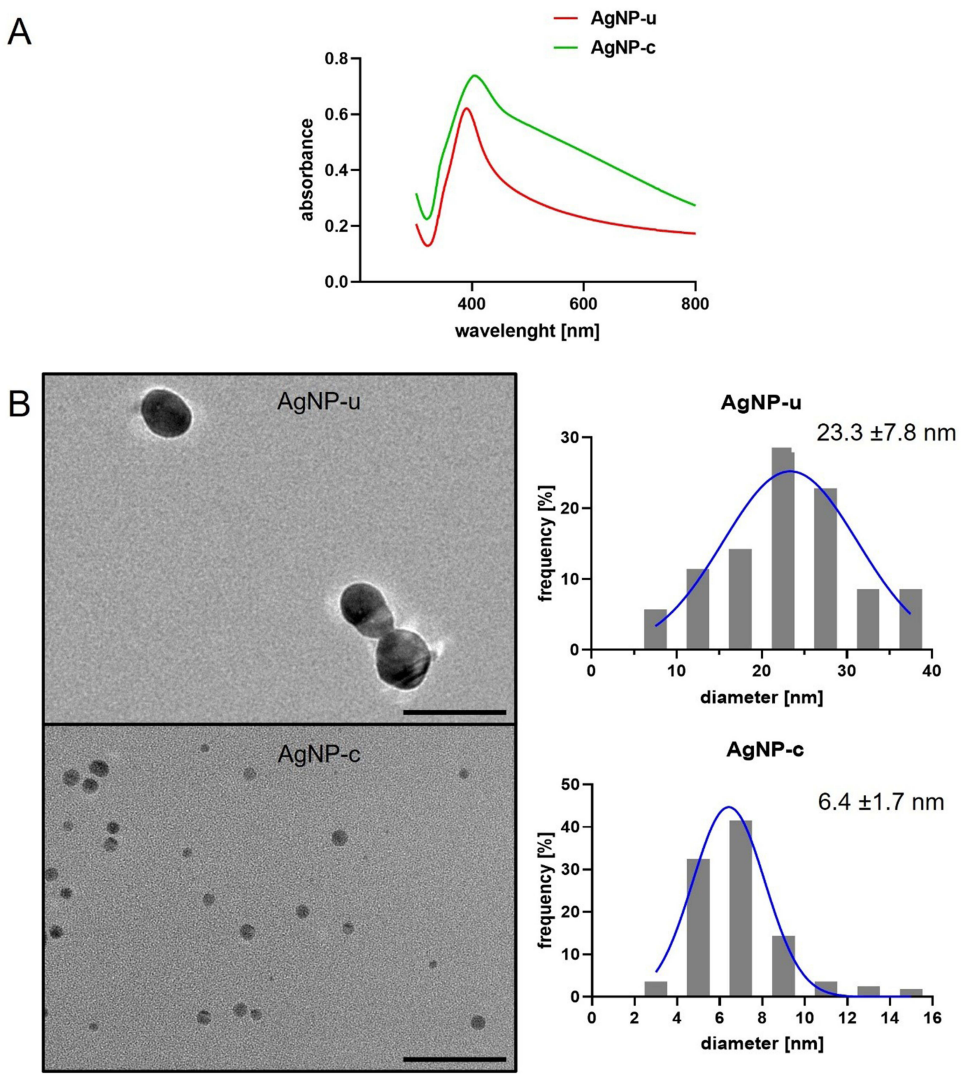

Figure 1 Characterization of AgNPs. (**A**) UV-Vis spectra of AgNPs-u and AgNPs-c showing the characteristic SPR absorbance peaks at 390 nm and 405 nm, respectively. (**B**) TEM images of both types of AgNPs and histograms of AgNP size distribution with an average size of 23.3 ±7.8 nm and 6.4 ±1.7 nm for AgNPs-u and AgNPs-c, respectively. Scale bars: 50 nm. AgNPs-u: uncapped silver nanoparticles, AgNPs-c: citrate-capped silver nanoparticles.

incorporate into the hydrophobic core of the lipid membrane. However, some interaction of AgNPs with the lipid membrane surface may be expected, which could affect encapsulation, stability and LAg properties.

With the intention to avoid the adverse effects of free AgNPs in future biomedical applications unencapsulated, free AgNPs were separated from LAgs by SEC. As shown in Figure 2A much of the brownish color indicating AgNPs were eluted in steps 1–5 together with larger-sized LAgs (left columns), while free AgNPs (right column) were entrapped at the top of the column. The presence and removal of free AgNPs are also evident from the DLS data of unpurified vs purified LAg samples (Figure 2B), with the important note that small-sized free AgNPs result in less intensive scattering as compared to liposomes of 100–150 nm size. Therefore the ratio of unencapsulated AgNPs is underestimated in the DLS plot. As shown in XRD spectra, the Ag signal was retained in LAg samples after purification (Supplementary Figure S1).[41] TEM images visually confirmed that significant fractions of AgNPs were found in and also out of unpurified liposomes (Figure 2C). After purification, free AgNPs were no longer visible, while encapsulated AgNPs could be seen in all types of LAgs irrespective of the AgNP type used (Figure 2D). In the following tests and experiments only purified LAgs were used, except when free AgNPs were applied as a control.

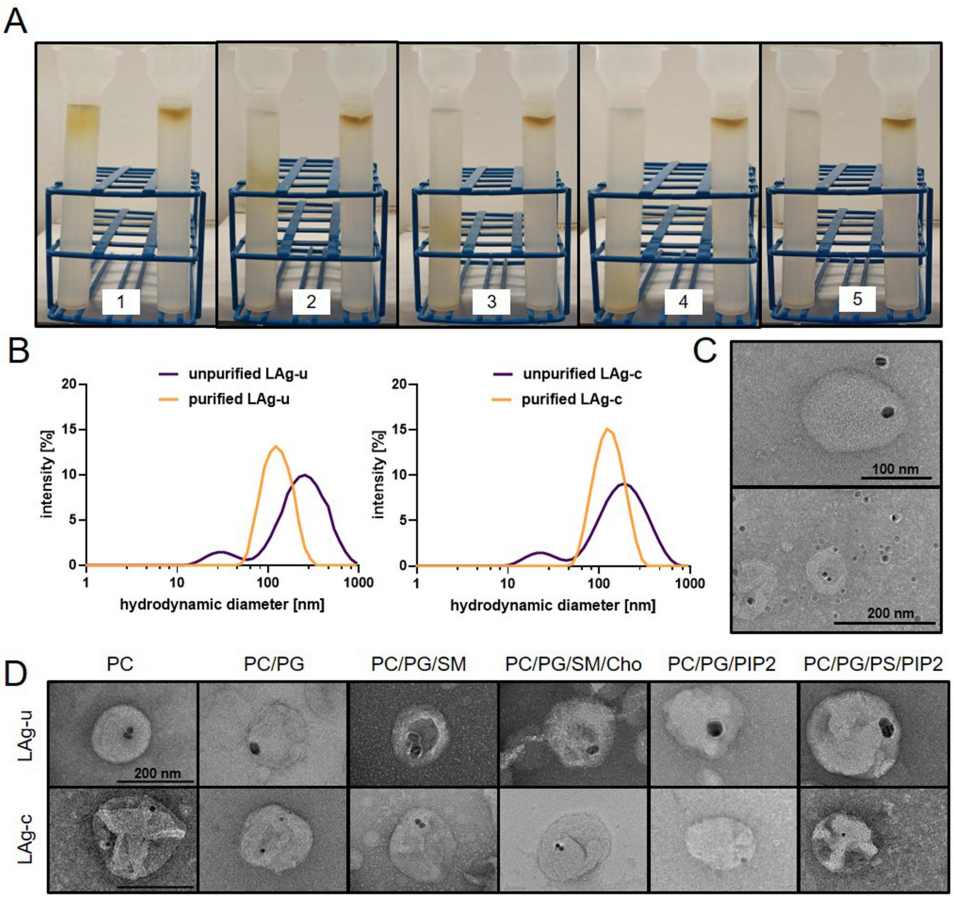

Figure 2 LAg purification and characterization. (**A**) The flow of LAg purification using SEC (shown for PC/PG-LAg-c). Both types of free, unencapsulated AgNPs were removed by Sephadex G-200. The left column was loaded with LAgs, while the right column was loaded with free AgNPs (without liposomes). Note that 1, 2, 3, 4 and 5 represent the sequential steps of sample elution. Fractions 4 and 5 positive for lipids were collected as purified LAgs. (**B**) DLS size distribution analysis of unpurified and purified PC/PG-LAgs-u and PC/PG-LAgs-c. Normalized curves display the removal of unencapsulated AgNPs. (**C**) TEM images of unpurified PC/PG-LAgs-c show AgNPs outside and inside the liposomes. Scale bars: 100 nm and 200 nm. (**D**) Different formulations of purified LAgs visualized by TEM. Scale bars: 200 nm.

LAg Properties and Biostability

Hydrodynamic diameters of LAgs were found to be in the range of 100–150 nm with some minor changes observed upon AgNP encapsulation (Table 2). The Zeta potential of liposomes was, however, considerably affected by AgNP encapsulation. Apart from the liposomes containing the highly negatively charged PIP2, Zeta values decreased, indicating that LAgs may be more stable, and less prone to aggregation than empty liposomes.

Table 2 Z-Average and Zeta Potential Values of Purified Liposomes Measured by DLS. Z-Average and Zeta Potential Data Describe the Hydrodynamic Diameter and Surface Charges of Liposomes, Respectively

Sample	Z-Average (nm)	Zeta Potential (mv)
PC	154.8	−7.9
PC-Ag-u	90.3	−20.0
PC-Ag-c	117.3	−18.1
PC/PG	108.7	−26.9

(*Continued*)

https://doi.org/10.2147/IJN.S498208

Table 2 (Continued).

Sample	Z-Average (nm)	Zeta Potential (mv)
PC/PG-Ag-u	106.0	−34.0
PC/PG-Ag-c	104.9	−37.8
PC/PG/SM	125.0	−23.0
PC/PG/SM-Ag-u	120.4	−36.0
PC/PG/SM-Ag-c	110.0	−31.0
PC/PG/SM/Cho	145.7	−29.5
PC/PG/SM/Cho-Ag-u	120.0	−40.0
PC/PG/SM/Cho-Ag-c	184.8	−34.5
PC/PG/PIP2	115.0	−42.0
PC/PG/PIP2-Ag-u	108.0	−39.0
PC/PG/PIP2-Ag-c	108.0	−45.0
PC/PG/PS/PIP2	123.0	−39.0
PC/PG/PS/PIP2-Ag-u	101.0	−41.0
PC/PG/PS/PIP2-Ag-c	152.3	−49.7

Notes: no sign, -Ag-u and -Ag-c labels represent empty liposomes (L), LAg-u and LAg-c, respectively.

To assess the rate of LAg filling, empty liposomes vs LAgs were loaded with CF and placed onto density gradients. In agreement with the assumption that LAgs are denser, empty liposomes remained at the very top of the gradient, while much of the LAg samples penetrated into denser gradient layers (Figure 3A: I, III, V). Meanwhile, the brownish color of

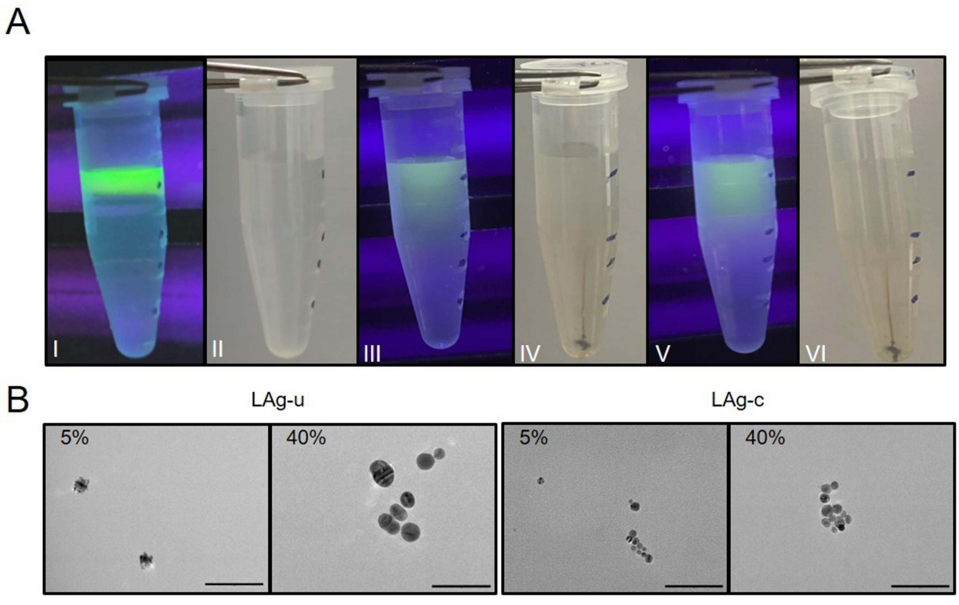

Figure 3 DGC fractionation and TEM analysis of LAgs. (**A**) Different DGC profiles for purified CF-loaded empty (**L**) vs Ag-liposomes (LAgs) under UV (**I**, III, (**V**) or at visible light (II, IV, VI) shown for empty PC-L (**I**, II), PC-Ag-u (III, IV) and PC-Ag-c (**V**, VI). (**B**) TEM images of the 5% and 40% DGC fractions of PC-LAg-u and PC-LAg-c. Note that liposomes were not visualized in these images. Scale bars: 50 nm.

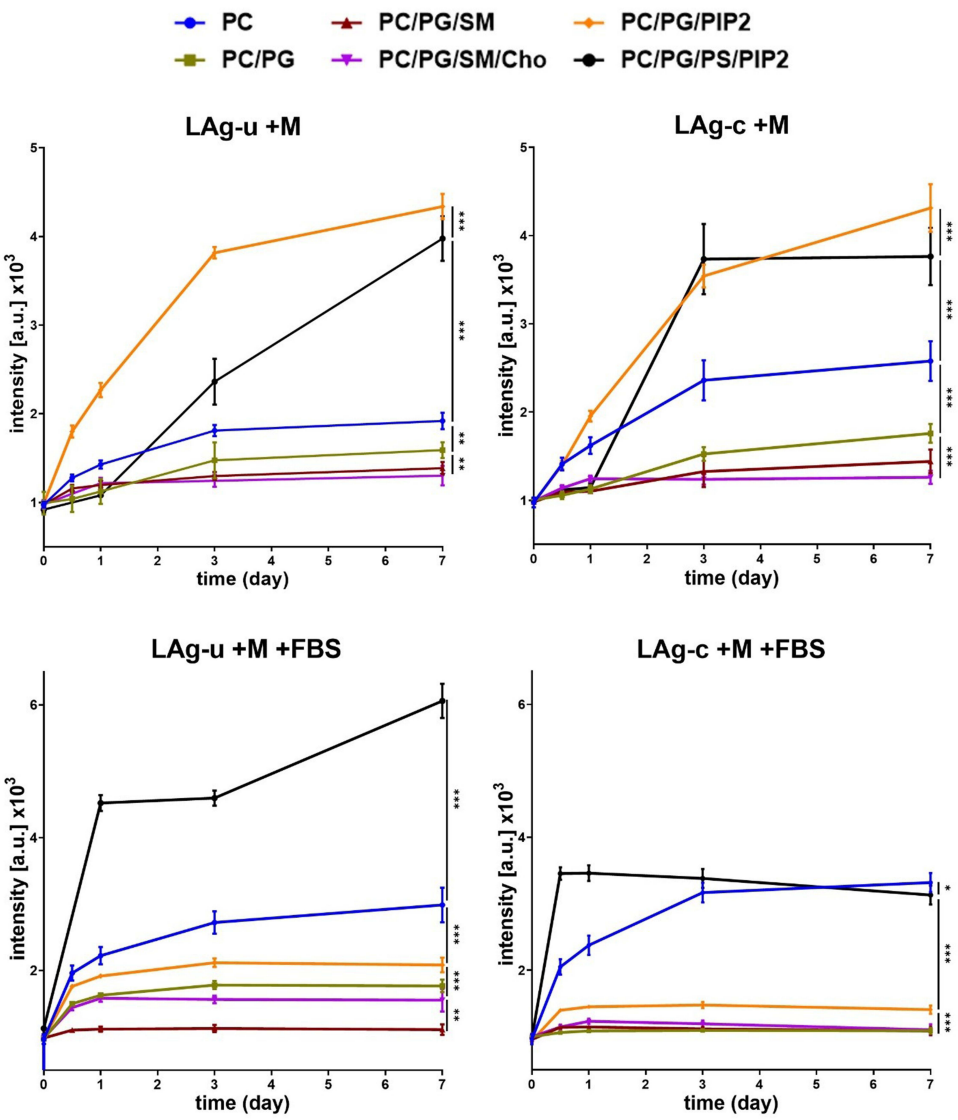

Figure 4 Differential stability of LAgs in biofluids. Purified CF-loaded LAgs-u and LAgs-c were incubated in DMEM (M) or in DMEM +10% FBS (M +FBS) at 37 °C for 7 days. Impairment of liposomal membrane integrity was monitored by CF leakage shown as relative increase in fluorescence compared to day 0 values. Note that CF fluorescence was not affected by the different biofluids used.
Notes: n= 8, and *p < 0.05, **p < 0.01, ***p < 0.001.

AgNP content of LAgs was visible in the denser gradient fractions, at least partly overlapping with the lipid stain pattern visualized (Figure 3A: II, IV, VI). Sedimentation of free AgNPs and AgNPs in LAgs were also clearly distinguishable, where LAgs penetrated into denser gradient layers (Supplementary Figure S2). It is worth noting that AgNPs encapsulated in liposomes may be less visible, which could hinder their observation. All these data pointed out that LAgs account for a considerable fraction of liposomes.

To further assess the properties of LAgs, the gradient layers were analyzed for their AgNP and lipid content. AgNPs of note could be detected even in the top gradient layer, although the majority of AgNP content appeared to be in the bottom fraction (Figure 3A: IV, VI and Figure 3B). As an attempt to screen for the most AgNP-loaded LAg formula, lipid contents of the gradient layers of different lipid compositions were measured. In most cases, no striking differences were seen (data not shown), but lipid accumulation was observed in denser gradient layers of PC-LAgs, and in particular those of PC/PG/SM-LAgs as compared to empty liposomes (Supplementary Figure S3). Nonetheless, the presence of AgNP content of LAgs even in the top gradient layers (Figure 3B) showed that this approach underestimates the extent of the AgNP-containing liposome fraction.

https://doi.org/10.2147/IJN.S498208

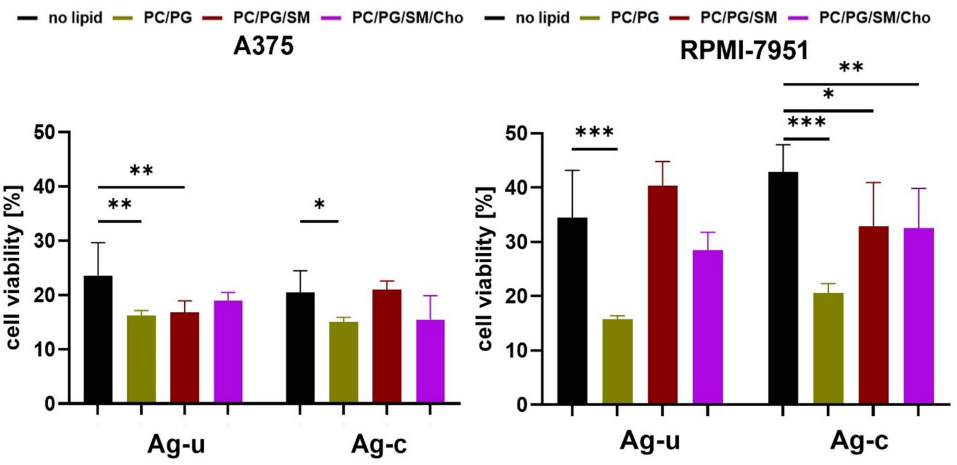

Figure 5 LAgs effectively reduce viability of melanoma cells. Viability of A375 and RPMI-7951 cells was measured by MTT assay upon exposure to AgNPs (no lipid) and different formulations of LAgs for 48 h. Cells were exposed to 0.5 μg/mL AgNPs, which is equivalent to the AgNP levels in LAgs at 30% EE. Data are expressed as relative to those of untreated control (AgNPs) or empty liposomes (LAgs). Note that the presence of empty liposomes did not affect viability significantly.
Notes: n= 6, and *p < 0.05, **p < 0.01, ***p < 0.001.

To ensure an effective LAg formulation that is suitable for low-toxic targeted therapy, the stability of LAgs was tested at different conditions. CF-loaded LAgs were kept in a medium that is isotonic to blood plasma or in a medium with FBS that was meant to mimic blood serum. At the initial time point after LAg purification, low fluorescence levels were measured due to self-quenching of CF present at high concentration inside the liposomes. Leaking of CF, displayed as an increase in fluorescence, was most pronounced for LAgs kept in water (data not shown). The neutral PC- and, in particular PIP2-containing negatively charged LAgs were leaking in medium as well, while PC/PG-, PC/PG/SM- and PC/PG/SM/Chol-LAgs were fairly stable at 37 °C for 7 days (Figure 4). Upon the addition of FBS, the highly charged PC/PG/PS/PIP2-LAgs and the neutral PC-LAgs were rapidly destabilized. As compared to medium conditions stability of PC/PG/PIP2-LAgs considerably improved in the presence of FBS, however PC/PG-, PC/PG/SM- and PC/PG/SM/Chol-LAgs proved to be the most stable at this condition as well (Figure 4). PC/PG- and PC/PG/SM/Cho-LAgs loaded with AgNPs-u were slightly leaking in the presence of FBS. In contrast, PC/PG- and PC/PG/SM/Cho-LAgs with AgNPs-c were fully stable PC/PG/SM-LAgs were the only LAg formulation that was found stable in the presence of FBS irrespective of the AgNP type loaded.

Purified LAgs Suppress Tumor Cell Viability

To test the antitumor activity of LAgs, the most stable purified AgNP-containing liposomes, PC/PG-, PC/PG/SM- and PC/PG/SM/Cho-LAgs were used in MTT viability assays. As determined by ICP-MS, encapsulation efficiencies (EEs) were found to be 18.7% and 25.5% in PC-LAgs, whereas 24.9% and 21.1% in PC/PG/SM-LAgs for LAg-u and LAg-c samples, respectively. Therefore, concentrations of free AgNPs equivalent to 30.0% encapsulation were used in comparison. It should be noted that this concentration of any free AgNPs (0.5 μg/mL) had a close to saturating effect on the viability of melanoma cells (Supplementary Figure S4). At these conditions used, LAgs and free AgNPs reduced the viability of A375 cells by around 80% as compared to their own empty vehicles (Figure 5). PC/PG- and PC/PG/SM-LAg-u and PC/PG-LAg-c were significantly more efficient than their free AgNP controls, while the other LAgs were similar to the controls. At the same time, the same level of LAgs and free AgNPs reduced the viability of RPMI-7951 cells by around 60% as compared to their own empty vehicles (Figure 5). PC/PG-LAg-u and all LAg-c resulted in a sizeable reduction in viability as compared to free AgNPs, while the other LAgs-u were not significantly different from the free AgNP-u control. It is of note that in comparison to free AgNPs, LAgs were less toxic to human embryonic kidney, HEK293 cells used as a non-cancerous control (Supplementary Figure S5). It is also noted that liposomes alone did not affect viability values (data not shown).

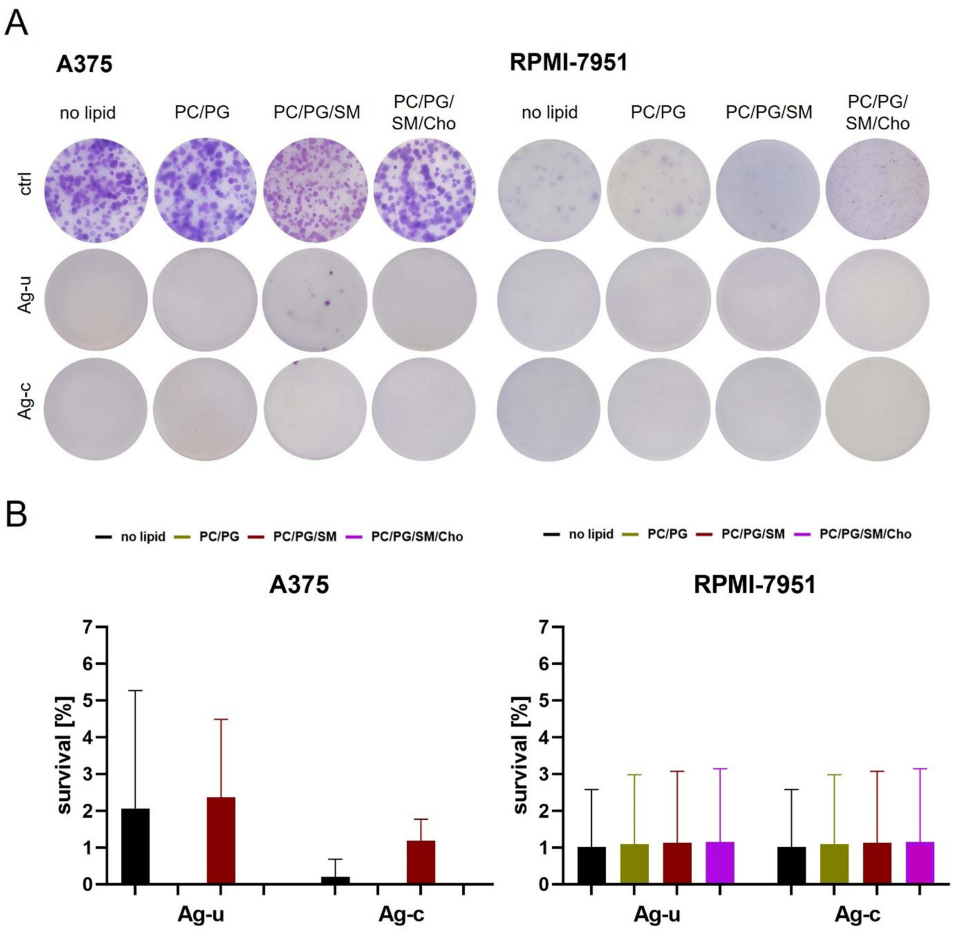

Figure 6 LAgs effectively block clonogenic potential of melanoma cells. Colony-forming ability of A375 and RPMI-7951 cells was monitored upon treatments with AgNPs (no lipid) or LAgs for 11 days. Cells were exposed to 0.5 μg/mL AgNPs, which is equivalent to the AgNP levels in LAgs at 30% EE. (**A**) Representative images of the fixed and stained colonies at day 11. (**B**) Data are based on manual counting of colonies and expressed as relative to those of untreated control (AgNPs) or empty liposomes (LAgs). Note that the presence of empty liposomes did not affect viability significantly.
Notes: n= 3.

To assess the longer-term effect of LAgs on tumor cell viability, the colony-forming ability of melanoma cells was also tested. As shown in Figure 6A, untreated A375 cells formed several colonies during the long-term experiment. Upon treatment with any free AgNPs, a dramatic inhibition of cell growth and survival was observed. Compared to their own empty vehicles, PC/PG- and PC/PG/SM/Chol-LAg-u had significantly more effect than their free AgNP control. Meanwhile, LAgs-c were equally efficient to their free AgNP control. Untreated RPMI-7951 cells formed viable but much smaller colonies, which were equally inhibited by either free AgNPs or any type of LAgs. Counting the number of colonies confirmed the results of visual inspection (Figure 6B) and pointed out a strong ability of LAgs to block survival of melanoma cells.

Purified LAgs Inhibit 3D Tumor Spheroid Invasion

As shown above, tumor cell viability could be strongly impaired by either free AgNPs or LAgs with some advantage of LAgs even without active targeting (see Figures 5 and 6). Even though PC/PG-LAgs appeared to have the highest antitumor effect their stability was slightly compromised in long-term tests (see Figure 4), therefore PC/PG/SM-LAgs were chosen for further long-term experiments. To assess the effectiveness of free AgNPs and LAgs in a tissue-like environment a 3D spheroid invasion assay was used. This experimental model involves a small tumor spheroid surrounded by Matrigel of a gel-like consistency, which resembles a simplified initial tumor spot. When free AgNPs were added to the tumor-surrounding gel, significant inhibition of A375 spheroid invasion was observed irrespective of

https://doi.org/10.2147/IJN.S498208

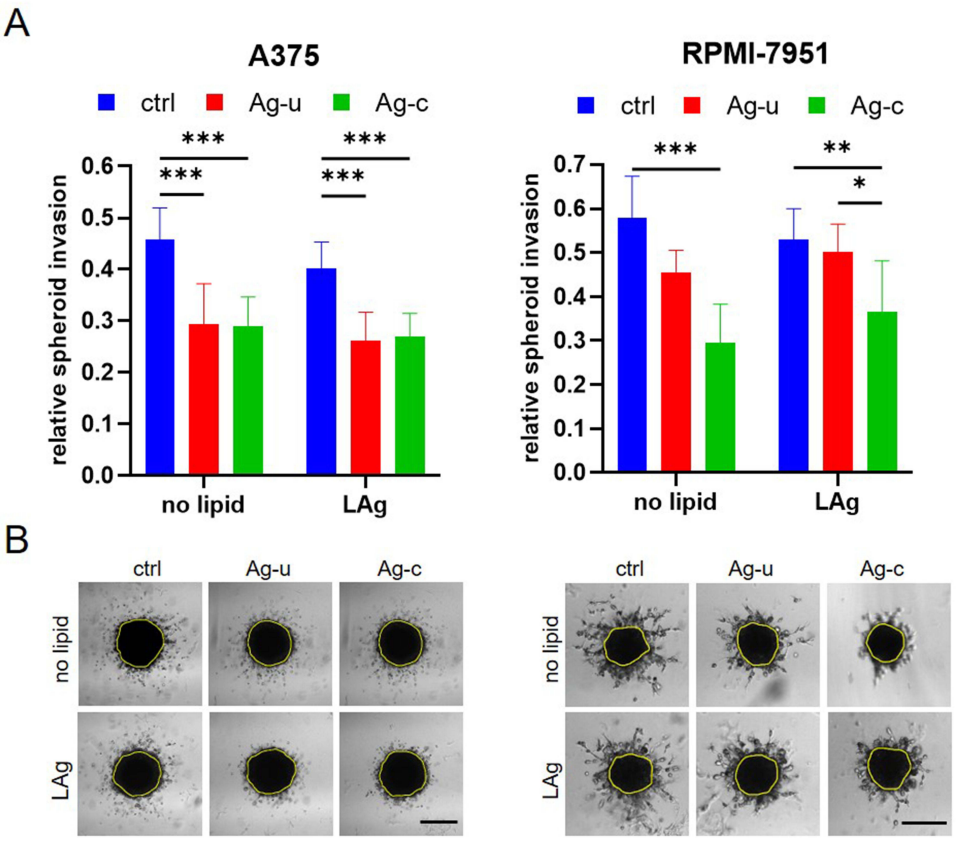

Figure 7 LAg-u and LAg-c differentially affect 3D spheroid invasion of melanoma cells. A375 and RPMI-7951 spheroids were embedded in Matrigel without (ctrl) or with AgNPs (no lipid), or with PC/PG/SM-LAgs (at 2.5 µg/mL Ag content), and growth and invasion were monitored by brightfield microscopy. Cross-sections of spheroids imaged 96 h after embedding were analyzed. (**A**) Extent of invasion, calculated as the yellow core area subtracted from the total spheroid area, are shown as relative to the initial size of spheroids at 0 h. (**B**) Representative images with the core area marked in yellow are shown. Scale bars are 500 and 300 µm for A375 and RPMI-7951 spheroids, respectively.
Notes: n= 6, and *p < 0.05, **p < 0.01, ***p < 0.001.

the AgNP type (Figure 7). Similar results were obtained when LAgs were tested. Interestingly, RPMI-7951 spheroids were not significantly affected by free AgNPs-u, however, their invasion was largely reduced by free AgNPs-c. In line with this, invasion of RPMI-7951 spheroids was impaired by LAg-c only. These data pointed out that both free AgNPs and LAgs could inhibit melanoma spheroid invasion, however, mesenchymally invading RPMI-7951 spheroids do not respond to AgNPs-u.

Discussion

AgNPs have been widely shown to have potential beneficial effects for the treatment of various diseases, which essentially relies on the cytotoxic ability. However, cytotoxicity of AgNPs is not limited to diseased cells,[42,43] therefore therapeutic use of AgNPs is hindered by potentially severe adverse effects. To overcome these challenges increasing efforts are made to encapsulate or entrap AgNPs in a NP format suitable for targeted applications. Attempts were made to apply organic coatings of AgNPs,[44] improving biocompatibility and reducing expected toxicity if specific targeting is provided.[45] In this study, a liposome-based encapsulation platform was introduced, which is highly biocompatible, ideal for co-administration of additional chemotherapeutic drugs and easily internalized to the target cell. In addition, encapsulated AgNPs are not directly coated hence they are more easily exposed at the proposed site of action. To make use of all these advantages of a liposome-based AgNP formulation in future applications, only purified LAgs, free of any unencapsulated AgNPs were tested for the first time, for their long-term stability and antitumor activity. By systematic analysis of a series of liposomes of different composition, loaded with different types of AgNPs, the LAg formulations of PC/PG, PC/PG/SM/Cho, and in particular PC/PG/SM were found very stable for AgNP delivery. These

LAgs, in particular PC/PG-LAgs even without active targeting were more efficient against tumor cells and less toxic to healthy controls as compared to free AgNPs, demonstrating another advantage of the liposomal formulation other than avoiding unwanted toxicity due to direct AgNP exposure. These lipid formulas of note are highly biocompatible and physiologically indifferent,[28] hence they appear ideal liposome carriers. It is also noteworthy that LAgs-c with smaller-sized AgNPs were more efficient than LAgs-u, therefore smaller encapsulated AgNPs appear to have higher antitumor activity probably due to their higher specific surface area. In agreement, this was also noticed with lipid-coated AgNPs, where smaller NPs were found to be more toxic.[46]

In our experimental settings LAgs were found denser than free AgNPs or empty liposomes, but a complete separation was not feasible by DGC. Purification of LAgs was therefore performed by SEC, and the EE of AgNPs into liposomes was determined by ICP-MS analysis of SEC-purified vs unpurified samples. 18.7 to 25.5% EE values were measured for PC- and PC/PG/SM-LAgs, which showed that a reasonable fraction of AgNPs were encapsulated in liposomes irrespective of the AgNP type or size. Importantly, these data also pointed out that LAg purification is essential in order to avoid adverse effects of a large fraction of free, unencapsulated AgNPs remained during preparation. Another aspect of LAgs that has not been addressed in previous studies is liposomal stability. Despite the highly negative Zeta potential of PS- and PIP2- containing LAgs these formulas were fairly unstable in different biofluids, possibly due to lipid head group interactions with medium and serum components. Zwitterionic PC-LAgs with a neutral surface were prone to aggregation, and liposomal leakage was also obvious. PC/PG-, PC/PG/SM- and PC/PG/SM/Cho-LAgs with a balanced lipid composition were shown to be stable Of these, PC/PG/SM-LAgs showed the highest stability, while during DGC their lipid densities were most affected by AgNP encapsulation. According to the DGC-based lipid content measurements, a minimum of 15.7% or 14.0% of the PC/PG/SM-LAgs contained AgNPs-u or AgNPs-c, respectively.

Free AgNP concentrations equivalent to 30% of EE levels in LAgs (0.5 μg/mL) greatly reduced the short-term viability and long-term clonogenic potential of melanoma cells. Depending on the lipid composition, LAgs with comparable (18.7 to 25.5%) levels of encapsulated AgNPs had significantly larger or at least similar effect on tumor and less effect on healthy cell viability, pointing out a benefit of passive targeting of liposomes with encapsulated AgNPs. This is probably due to the well-known enhanced internalization and turnover of tumor cells. Furthermore, upon active targeting purified LAgs are expected to show even stronger antitumor effects due to specific recognition and uptake of LAgs.[33] In a diffusion-limited gel-embedded 3D spheroid tumor invasion model the most stable but untargeted PC/PG/SM-LAgs were found as effective as free AgNPs. Interestingly, both 2D viability and 3D invasion experiments differentiated between AgNP types, suggesting that overcoming diffusion limitations by providing active targeting could further improve the effectiveness of LAgs. The difference between the effectiveness of Ag-u/LAg-u and Ag-c/LAg-c may be explained by the smaller sizes of AgNPs-c,[47] or by a more selective effect of AgNPs-c on mesenchymally (RPMI-7951) vs amoeboid (A375) invading tumor cells.[48] Taken together, in this study we encapsulated toxic AgNPs in liposome-based nanocarriers that are suitable for multimodal targeted therapies. Multiple lines of evidence are provided that AgNPs were incorporated into various liposomes, from which PC/PG/SM-LAgs are shown to be the most stable for AgNP delivery at physiologically relevant conditions. As compared to free AgNPs, untargeted PC/PG-, PC/PG/SM and PC/PG/SM/Chol-LAgs are shown to effectively reduce tumor cell viability and 3D tumor invasion, therefore are proposed as NP platforms for the development of various targeted LAg tumor therapies.

Conclusion

AgNPs have great potential for antitumor therapy, however their universal toxicity needs to be controlled and directed by advanced nanoparticle formulations specifically targeted towards the diseased tissue. For the first time, we have made a systematic study to unravel the physicochemical properties such as stability of purified liposome-encapsulated AgNPs (LAgs) at biorelevant conditions. Selected LAgs were proven to be effective against viability, clonogenic potential and even 3D tissue-like invasion of cancer cells. Purified LAgs, which contained no free AgNPs, were in part more effective against tumor cells than free AgNPs, suggesting that lipid encapsulation itself could improve the effectiveness of AgNPs. LAgs prepared in our study could be loaded with any drug candidates, and via any desirable targeting of the liposomes they allow specific, non-toxic and efficient treatment of tumor cells. These findings therefore hold the promise to further advance the development of combined antitumor nanoparticles based on AgNPs.

Abbreviations

AgNPs, silver nanoparticles; AgNPs-c, citrate-stabilized silver nanoparticles; AgNPs-u; uncapped silver nanoparticles; ANS, anilinonaphthalene-8-sulfonic acid; CF, carboxyfluorescein; Cho, cholesterol; DGC, density gradient centrifugation; DLS, dynamic light scattering; DMEM, dulbecco's modified eagle medium; DOPC, 1.2-dioleoyl-sn-glycero -3-phosphocholine; DOPG, 1.2-dioleoyl-sn-glycero-3-phospho-glycerol; DOPS, 1.2-dioleoyl-sn-glycero-3-phospho-L-serine; DPPC, dipalmitoylphosphatidylcholine; DSPC, distearylphosphatidylcholine; EE, encapsulation efficiency; FBS, fetal bovine serum ultra-low endotoxin; LAg, Ag-liposome; LUVs, large unilamellar vesicles; MTT, 3-(4,5-dimethylthiazol-2-yl)-2,5-diphenyltetrazolium bromide; MPS, mononuclear phagocyte system; NPs, nanoparticles; PIP2, phosphatidylinositol 4.5-biphosphate; ROS, reactive oxygen species; SEC, size exclusion chromatography; SM, N-palmitoyl-D-sphingomyelin; SPR, surface plasmon resonance; TEM, transmission electron microscope; UA, uranyl acetate.

Acknowledgment

Z.B. is a János Bolyai research fellow with a research program on "Human tumor patterns" (bo_198_21) and is supported by ÚNKP-23-5-PTE-2170, New National Excellence Program of the Ministry for Culture and Innovation from the source of National Research, Development and Innovation Fund. Funding from TKP2021-EGA-17 (F.G.jr.) of the National Research, Development and Innovation Office, Ministry for Innovation and Technology is acknowledged. This publication is based upon work from COST Action Pan-European Network in Lipidomics and EpiLipidomics (EpiLipidNET), CA19105, supported by COST (European Cooperation in Science and Technology).

Disclosure

The authors report no conflicts of interest in this work.

References

1. Alrushaid N, Khan FA, Al-Suhaimi EA, Elaissari A. Nanotechnology in cancer diagnosis and treatment. *Pharmaceutics*. 2023;15(3):1025. doi:10.3390/pharmaceutics15031025
2. Patra JK, Das G, Fraceto LF, et al. Nano based drug delivery systems: recent developments and future prospects. *J Nanobiotechnol*. 2018;16 (1):1–33. doi:10.1186/s12951-017-0328-8
3. Lee SH, Jun B-H. Silver nanoparticles: synthesis and application for nanomedicine. *Int J mol Sci*. 2019;20(4):865. doi:10.3390/ijms20040865
4. Cavassin ED, de Figueiredo LFP, Otoch JP, et al. Comparison of methods to detect the in vitro activity of silver nanoparticles (AgNP) against multidrug resistant bacteria. *J Nanobiotechnol*. 2015;13(1):1–16. doi:10.1186/s12951-015-0120-6
5. Fong J, Wood F, Fowler B. A silver coated dressing reduces the incidence of early burn wound cellulitis and associated costs of inpatient treatment: comparative patient care audits. *Burns*. 2005;31(5):562–567. doi:10.1016/j.burns.2004.12.009
6. Haggag EG, Elshamy AM, Rabeh MA, et al. Antiviral potential of green synthesized silver nanoparticles of Lampranthus coccineus and Malephora lutea. *Int J Nanomed*. 2019;Volume 14:6217–6229. doi:10.2147/IJN.S214171
7. Hashem AH, Saied E, Amin BH, et al. Antifungal activity of biosynthesized silver nanoparticles (AgNPs) against aspergilli causing aspergillosis: ultrastructure study. *J Funcl Biomat*. 2022;13(4):242. doi:10.3390/jfb13040242
8. He W, Zhou Y-T, Wamer WG, Boudreau MD, Yin -J-J. Mechanisms of the pH dependent generation of hydroxyl radicals and oxygen induced by Ag nanoparticles. *Biomaterials*. 2012;33(30):7547–7555. doi:10.1016/j.biomaterials.2012.06.076
9. Liu J, Zhao Y, Guo Q, et al. TAT-modified nanosilver for combating multidrug-resistant cancer. *Biomaterials*. 2012;33(26):6155–6161. doi:10.1016/j.biomaterials.2012.05.035
10. Liu Z, Tan H, Zhang X, et al. Enhancement of radiotherapy efficacy by silver nanoparticles in hypoxic glioma cells. *Artificial cells, nanomedicine, and biotechnology. Gynecol Obstet Fertil Senol*. 2018;46(sup3):922–930. doi:10.1016/j.gofs.2018.10.027
11. Kovács D, Szőke K, Igaz N, et al. Silver nanoparticles modulate ABC transporter activity and enhance chemotherapy in multidrug resistant cancer. *Nanomed Nanotechnol Biol Med*. 2016;12(3):601–610. doi:10.1016/j.nano.2015.10.015
12. Yang E-J, Kim S, Kim JS, Choi I-H. Inflammasome formation and IL-1β release by human blood monocytes in response to silver nanoparticles. *Biomaterials*. 2012;33(28):6858–6867. doi:10.1016/j.biomaterials.2012.06.016
13. Patlolla AK, Hackett D, Tchounwou PB. Silver nanoparticle-induced oxidative stress-dependent toxicity in Sprague-Dawley rats. *mol Cell Biochem*. 2015;399(1–2):257–268. doi:10.1007/s11010-014-2252-7
14. Rohde MM, Snyder CM, Sloop J, et al. The mechanism of cell death induced by silver nanoparticles is distinct from silver cations. *Particle Fibre Toxicol*. 2021;18(1):1–24. doi:10.1186/s12989-021-00430-1
15. Olugbodi JO, Lawal B, Bako G, et al. Effect of sub-dermal exposure of silver nanoparticles on hepatic, renal and cardiac functions accompanying oxidative damage in male Wistar rats. *Sci Rep*. 2023;13(1):10539. doi:10.1038/s41598-023-37178-x
16. Ahamed M, Karns M, Goodson M, et al. DNA damage response to different surface chemistry of silver nanoparticles in mammalian cells. *Toxicol Appl Pharmacol*. 2008;233(3):404–410. doi:10.1016/j.taap.2008.09.015

17. Kovács D, Igaz N, Keskeny C, et al. Silver nanoparticles defeat p53-positive and p53-negative osteosarcoma cells by triggering mitochondrial stress and apoptosis. *Sci Rep*. 2016;6(1):27902. doi:10.1038/srep27902
18. Yang T, Yao Q, Cao F, Liu Q, Liu B, Wang X-H. Silver nanoparticles inhibit the function of hypoxia-inducible factor-1 and target genes: insight into the cytotoxicity and antiangiogenesis. *Int J Nanomed*. 2016;Volume 11:6679–6692. doi:10.2147/IJN.S109695
19. Yang L, Kuang H, Zhang W, Aguilar ZP, Wei H, Xu H. Comparisons of the biodistribution and toxicological examinations after repeated intravenous administration of silver and gold nanoparticles in mice. *Sci Rep*. 2017;7(1):3303. doi:10.1038/s41598-017-03015-1
20. Huang H, Lai W, Cui M, et al. An evaluation of blood compatibility of silver nanoparticles. *Sci Rep*. 2016;6(1):1–15. doi:10.1038/s41598-016-0001-8
21. Shrivastava S, Bera T, Singh SK, Singh G, Ramachandrarao P, Dash D. Characterization of antiplatelet properties of silver nanoparticles. *ACS nano*. 2009;3(6):1357–1364. doi:10.1021/nn900277t
22. Liao C, Li Y, Tjong SC. Bactericidal and cytotoxic properties of silver nanoparticles. *Int J mol Sci*. 2019;20(2):449. doi:10.3390/ijms20020449
23. Alessandrini F, Vennemann A, Gschwendtner S, et al. Pro-inflammatory versus immunomodulatory effects of silver nanoparticles in the lung: the critical role of dose, size and surface modification. *Nanomaterials*. 2017;7(10):300. doi:10.3390/nano7100300
24. Miranda RR, Sampaio I, Zucolotto V. Exploring silver nanoparticles for cancer therapy and diagnosis. *Colloids Surf Biointer*. 2022;210:112254. doi:10.1016/j.colsurfb.2021.112254
25. Locatelli E, Broggi F, Ponti J, et al. Lipophilic silver nanoparticles and their polymeric entrapment into targeted-PEG-based micelles for the treatment of glioblastoma. *Adv Healthcare Mater*. 2012;1(3):342–347. doi:10.1002/adhm.201100047
26. Liu P, Chen G, Zhang J. A review of liposomes as a drug delivery system: current status of approved products, regulatory environments, and future perspectives. *Molecules*. 2022;27(4):1372. doi:10.3390/molecules27041372
27. Dymek M, Sikora E. Liposomes as biocompatible and smart delivery systems–The current state. *Adv Colloid Interface Sci*. 2022;309:102757. doi:10.1016/j.cis.2022.102757
28. Nsairat H, Khater D, Sayed U, Odeh F, Al Bawab A, Alshaer W. Liposomes: structure, composition, types, and clinical applications. *Heliyon*. 2022;8(5):e09394. doi:10.1016/j.heliyon.2022.e09394
29. Rost N, Sen K, Savliwala S, et al. Magnetic particle imaging performance of liposomes encapsulating iron oxide nanoparticles. *J Magn Magn Mater*. 2020;504:166675. doi:10.1016/j.jmmm.2020.166675
30. Jayachandran P, Ilango S, Suseela V, et al. Green synthesized silver nanoparticle-loaded liposome-based nanoarchitectonics for cancer management: in vitro drug release analysis. *Biomedicines*. 2023;11(1):217. doi:10.3390/biomedicines11010217
31. Liu J, Li X, Liu L, Bai Q, Sui N, Zhu Z. Self-assembled ultrasmall silver nanoclusters on liposome for topical antimicrobial delivery. *Colloids Surf Biointer*. 2021;200:111618. doi:10.1016/j.colsurfb.2021.111618
32. Yusuf A, Brophy A, Gorey B, Casey A. Liposomal encapsulation of silver nanoparticles enhances cytotoxicity and causes induction of reactive oxygen species-independent apoptosis. *J Appl Toxicol*. 2018;38(5):616–627. doi:10.1002/jat.3566
33. Skora B, Piechowiak T, Szychowski KA. Epidermal Growth Factor-labeled liposomes as a way to target the toxicity of silver nanoparticles into EGFR-overexpressing cancer cells in vitro. *Toxicol Appl Pharmacol*. 2022;443:116009. doi:10.1016/j.taap.2022.116009
34. Moors E, Sharma V, Tian F, Javed B. Surface-modified silver nanoparticles and their encapsulation in liposomes can treat MCF-7 breast cancer cells. *J Funcl Biomat*. 2023;14(10):509. doi:10.3390/jfb14100509
35. Bothun GD. Hydrophobic silver nanoparticles trapped in lipid bilayers: size distribution, bilayer phase behavior, and optical properties. *J Nanobiotechnol*. 2008;6(1):1–10. doi:10.1186/1477-3155-6-13
36. Allen TM, Hansen C, Rutledge J. Liposomes with prolonged circulation times: factors affecting uptake by reticuloendothelial and other tissues. *Biochim Biophys Acta*. 1989;981(1):27–35. doi:10.1016/0005-2736(89)90078-3
37. Badawy AME, Luxton TP, Silva RG, Scheckel KG, Suidan MT, Tolaymat TM. Impact of environmental conditions (pH, ionic strength, and electrolyte type) on the surface charge and aggregation of silver nanoparticles suspensions. *Environ Sci Technol*. 2010;44(4):1260–1266. doi:10.1021/es902240k
38. Bélteky P, Rónavári A, Igaz N, et al. Silver nanoparticles: aggregation behavior in biorelevant conditions and its impact on biological activity. *Int J Nanomed*. 2019;Volume 14:667–687. doi:10.2147/IJN.S185965
39. Marosvölgyi T, Mintál K, Farkas N, et al. Antibiotics and probiotics-induced effects on the total fatty acid composition of feces in a rat model. *Sci Rep*. 2024;14(1):6542. doi:10.1038/s41598-024-57046-6
40. Riss TL, Moravec RA, Niles AL, et al. Cell viability assays. *Assay Guidance Manual*. 2016 [Internet].
41. Ibrahim S, Ahmad Z, Manzoor MZ, Mujahid M, Faheem Z, Adnan A. Optimization for biogenic microbial synthesis of silver nanoparticles through response surface methodology, characterization, their antimicrobial, antioxidant, and catalytic potential. *Sci Rep*. 2021;11(1):770. doi:10.1038/s41598-020-80805-0
42. Sokołowska P, Białkowska K, Siatkowska M, et al. Human brain endothelial barrier cells are distinctly less vulnerable to silver nanoparticles toxicity than human blood vessel cells: a cell-specific mechanism of the brain barrier? *Nanomed Nanotechnol Biol Med*. 2017;13(7):2127–2130. doi:10.1016/j.nano.2017.05.015
43. Recordati C, De Maglie M, Bianchessi S, et al. Tissue distribution and acute toxicity of silver after single intravenous administration in mice: nano-specific and size-dependent effects. *Particle Fibre Toxicol*. 2015;13(1):1–17. doi:10.1186/s12989-016-0124-x
44. Sharma VK, Siskova KM, Zboril R, Gardea-Torresdey JL. Organic-coated silver nanoparticles in biological and environmental conditions: fate, stability and toxicity. *Adv Colloid Interface Sci*. 2014;204:15–34. doi:10.1016/j.cis.2013.12.002
45. Wang Y, Newell BB, Irudayaraj J. Folic acid protected silver nanocarriers for targeted drug delivery. *J Biomed Nanotechnol*. 2012;8(5):751–759. doi:10.1166/jbn.2012.1437
46. Lira CN, Carpenter AP, Baio JE, Harper BJ, Harper SL, Mackiewicz MR. Size-and shape-dependent interactions of lipid-coated silver nanoparticles: an improved mechanistic understanding through model cell membranes and in vivo toxicity. *Chem Res Toxicol*. 2024;37(6):968–980. doi:10.1021/acs.chemrestox.4c00053
47. Miethling-Graff R, Rumpker R, Richter M, et al. Exposure to silver nanoparticles induces size-and dose-dependent oxidative stress and cytotoxicity in human colon carcinoma cells. *Toxicol Vitro*. 2014;28(7):1280–1289. doi:10.1016/j.tiv.2014.06.005
48. Sur I, Altunbek M, Kahraman M, Culha M. The influence of the surface chemistry of silver nanoparticles on cell death. *Nanotechnology*. 2012;23(37):375102. doi:10.1088/0957-4484/23/37/375102